Journal of Photochemistry and Photobiology A: Chemistry 214 (2010) 203–214

Contents lists available at ScienceDirect

Journal of Photochemistry and Photobiology A: Chemistry

journal homepage: www.elsevier.com/locate/jphotochem

Lactim–lactam tautomerism is favoured over enol–keto tautomerism in 2-hydroxy-5-(4-fluorophenyl)nicotinic acid: Experimental and quantum chemical approach

Bijan Kumar Paul, Anuva Samanta, Samiran Kar, Nikhil Guchhait*

Department of Chemistry, University of Calcutta, 92 A.P.C. Road, Kolkata 700009, India

ARTICLE INFO

Article history:
Received 8 March 2010
Received in revised form 19 May 2010
Accepted 25 June 2010
Available online 22 July 2010

Keywords:
Competition between lactim–lactam and enol–keto tautomerism
2-Hydroxy-5-(4-fluorophenyl)nicotinic acid
Absorption and emission spectroscopy
DFT

ABSTRACT

A model compound, 2-hydroxy-5-(4-fluorophenyl)nicotinic acid (HFPNA) has been synthesized and its ground and excited-state properties towards tautomerisation via possible two ways of proton transfer process have been elaborately examined by means of steady-state absorption, emission and time-resolved emission spectroscopy and quantum chemical calculations. The theme issue of the present contribution is to illustrate a direct competition between two potential excited-state intramolecular proton transfer (ESIPT) pathways within the same molecule. By a direct comparison of spectral characteristics of HFPNA with those of salicylic acid (SA) and 2-hydroxypyridine (2HP) under similar experimental conditions it has been demonstrated that lactim–lactam tautomerisation dominates over enol–keto tautomerisation in HFPNA. Experimental evidences and structural calculation at Density Functional Theory (DFT) (B3LYP/6-31G**) and Hartree–Fock (6-31G**) levels predict the existence of both lactim and lactam-forms in the ground state. The ground and excited-state theoretical potential energy surfaces (PES) of HFPNA along both the ways of proton transfer coordinate at DFT level reveal that PES of HFPNA resemble well with that of 2HP while there are prominent differences from that of SA. We also report on the possibility of application of the studied molecule as a sensor of medium-pH following its sensitive response towards pH of the medium.

1. Introduction

The pioneering works of Weber [1], Förster [2] and Weller [3] envisaged a new arena of research in the field of photochemistry in the middle of the last century through the unique observation of Excited-State Intramolecular Proton Transfer (ESIPT) reaction in methyl salicylate. Since then this phenomenon has undergone an explosive growth by virtue of its promising roles in an extensive arena of research, providing the wide scope of important applications of ESIPT reaction. The unique four-level photophysical scheme of PT reaction normally allows the total exclusion of self-absorption (through rupture of mirror image symmetry between absorption/excitation and emission spectra) whereby promoting its application as ultraviolet stabilizers [4], laser dyes [5,6], radiation hard scintillators and so forth [7]. Furthermore, the ESIPT phenomenon has been exploited as optical probes for biomolecules and in the investigation of various biomimicking, biological and supramolecular microenvironments [8,9]. The attention focused on this phenomenon has thus, quite naturally, received immense stimulate not only because of its attractive photophysics but also for its conquer of a commanding position in applied research.

Salicylic acid (SA), the benchmark molecule studied vastly by different groups, shows ESIPT reaction via the pre-existing intramolecular six member hydrogen bond (IMHB) in the ground state. There are systems where the size of the hydrogen bonded ring is different from six member ring and sometimes intermolecular solvent mediated hydrogen bonding can assist the proton transfer process. An asymmetric double well type potential is modeled to describe the feasibility of proton transfer reaction for the ground and excited states for several prototype systems [10]. The proton transferred (PT) or the keto tautomer enormously differs from its corresponding enol tautomer in structure, charge density distribution and dipole moment and hence gives rise to a large Stokes shifted fluorescence, which is recognized as the "*spectroscopic signature*" of the process. The nature of the entire ESIPT process is found to be controlled by the barrier energy. Theoretically it is reported that low barrier or barrierless proton transfer process is the governing factor behind such ultrafast ESIPT reaction [10–12].

Similarly, another ESIPT system that has received huge attention over the years in the scientific community is 2-hydroxypyridine (2HP), which exhibits two stable tautomeric forms, the lactim-form

* Corresponding author. Tel.: +91 33 2350 8386; fax: +91 33 2351 9755.
E-mail addresses: nguchhait@yahoo.com, nikhil.guchhait@rediffmail.com (N. Guchhait).

1010-6030/$ – see front matter © 2010 Elsevier B.V. All rights reserved.
doi:10.1016/j.jphotochem.2010.06.028

2-hydroxypyridine (2HP) and the lactam-form 2-pyridone (2PY). A large volume of experimental and theoretical works have been pursued so far on the well-known ESIPT system of 2HP and the existence of both the tautomers at the ground state has been documented with the fact that 2HP is more stable than 2PY [13–34]. In fact, 2HP ↔ 2PY tautomerisation reaction has been enormously studied in various phases [13–21], in matrixes [22,23], while a massive volume of theoretical investigation has also been dedicated to the study of this system with special emphasis being driven to the concept of mimicking the system for mutation in DNA base pairs [24–28]. Experiments reveal that the enthalpy difference between 2HP and 2PY is 2–3 kJ/mol and hence 2HP form favours over 2PY-form and the barrier for conversion is 40–46 kcal/mol [29,30]. However, the latter form is known to predominate in polar solvents [29,30]. It is reported that the 2HP to 2PY tautomerisation via ESIPT process is controlled by the nature of the barrier, but it is quite interesting to note that DFT methods predict that in the ground state 2PY is more stable than 2HP [29–31]. Only methods including high electron correlation effects have been reported to be able to reproduce the experimental findings correctly [31–33]. A report of DFT energetic results indicates that 2PY is more stable than 2HP by 0.47 kcal/mol at DFT//B3LYP/6-311++G** level [31]. In spite of such discrepancy with the experimental results, DFT/B3LYP method has been quite appreciably exploited by several authors for the study of potential energy surface (PES), barrier height for 2HP ↔ 2PY transformation reaction with commendable efficiency and fruition [24–29,35,36].

In the present work, we have synthesized a new model molecule, 2-hydroxy-5-(4-fluorophenyl)nicotinic acid (HFPNA) and carried out a detailed photophysical study of the molecule based on spectroscopic techniques. The molecule is an important synthetic precursor for the synthesis of compounds having anxiolytic activity. Thus quite naturally a detailed photophysical characterization of the molecule is expected to exert positive impetus to its future applications through an improved understanding of its behaviour. Apart from this, a great many number of nicotinic acid derivatives has found enormous medicinal and biochemical applications since years [37a–c]. So quite naturally, studies designed to delve into the photophysical characterization of such important nicotinic acid derivatives demand relevance as well as significance with a view to improve their future applications through a more scrupulous characterization of their photophysics and photochemistry. Also the presence of the fluorine atom in HFPNA (Scheme 1) induces some quite critical but interesting modifications to the fundamental photophysics of the molecule through rendering the 4-fluorophenyl moiety electron deficient which subsequently paves way for explicit investigation on photoinduced electron transfer (PET) mechanism and its perturbation by various external agents [37d,e]. Modulations of photophysical properties of HFPNA imparted by external agents like protons, metal ions, etc. dictate its viable nature towards development of a new fluorescent chemosensor. However, with an emphasis on the target of our present work we avoid to comment on this topic in the present contribution. The structure of the molecule is crucial and quite interesting as it consists of two proton transfer sites suitable for tautomerisation, one resembles to SA and another resembles to 2HP. The co-existence of two very well known and suitable sites for ESIPT reaction in HFPNA paves the way for direct competition between the two routes of ESIPT making its photophysics quite complicated and challenging. The possibility of photoinduced electron

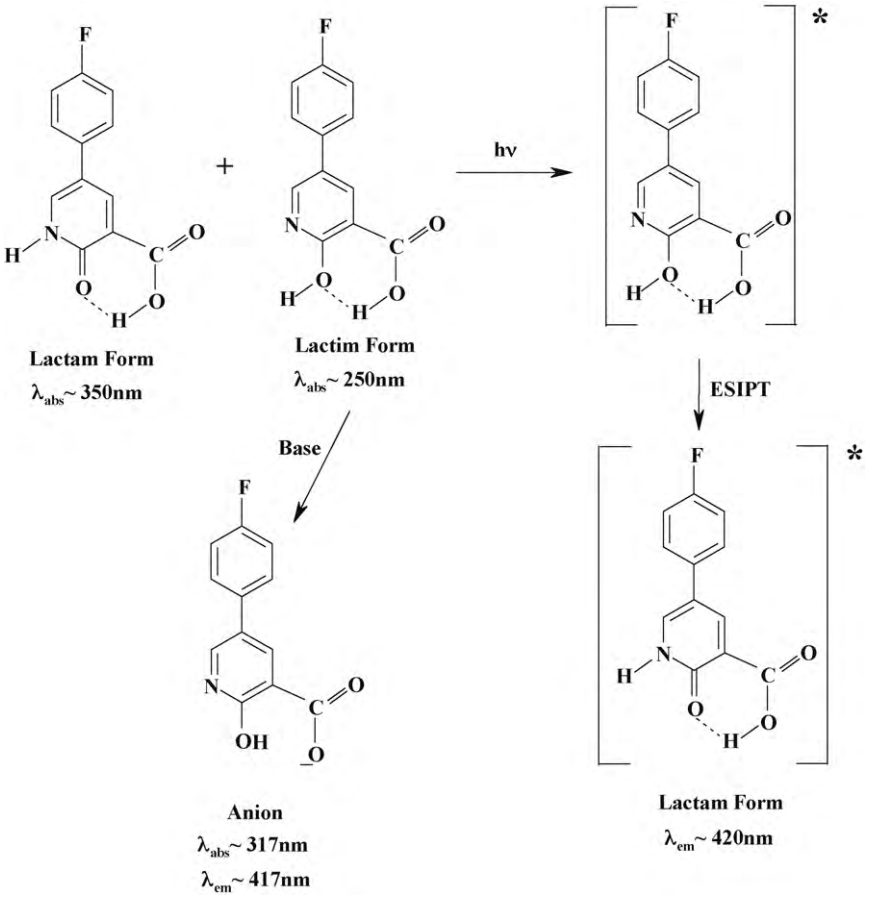

Scheme 1. Schematic presentation of ESIPT reaction (lactim–lactam tautomerisation) and different absorbing and emitting species of HFPNA.

transfer (PET) from the parent pyridine unit to electron deficient fluorophenyl unit can also have a possibility to compete with the PT reaction. As long as the occurrence of ESIPT reaction in both SA [38] and 2HP [29,39] is established, the study of photophysics of HFPNA will throw light into the direct competition between the two well-known ESIPT routes. Ground and excited-state properties have been explored using steady-state absorption and emission spectroscopy and time-resolved emission spectroscopy. At the same time quantum chemical calculations have also been performed in order to provide a theoretical support to our experimental findings. Structures, energies and potential energy curve (PEC) along the PT coordinate by quantum chemical calculations for the ground and excited states have been performed at Density Functional Theory (DFT) and Hartree–Fock (HF) levels of theory.

With a view to the swelling volume of reports available in literature concerning ground- and excited-state proton transfer reaction in numerous molecular systems, the present contribution seems to demand novelty in view of the critical but unique molecular architecture of the title compound HFPNA which subsequently leads to focus on an interesting issue: competition between two potential ESIPT pathways within the same molecule. As far as our knowledge goes, this is the first report of its kind.

2. Experimental

2.1. Synthesis of HFPNA

To a solution of the Vilsmeier reagent prepared from DMF and $POCl_3$ at 10 °C, 4-fluorophenyl acetic acid was added and then the mixture was stirred and heated at 70 °C for 8 h. After cooling to room temperature the mixture was added slowly to a mixture of ice and water (temperature <10 °C) and then a solution of Na_2CO_3 was added slowly until pH 11 was achieved. Toluene was added to the alkaline mixture and the resulting mixture was refluxed for 1.5 h. After cooling to room temperature the separated aqueous layer was extracted with toluene. The combined organic extracts were washed with water and dried Na_2SO_4 and toluene was evaporated in vacuo. The solid residue was recrystallized from the mixture of DCM and n-heptane to yield yellow crystals of 3-dimethylamino-2-(4-fluorophenyl)propenal.

To a solution of sodium methoxide in methanol, cyanoacetamide and 3-dimethylamino-2-(4-fluorophenyl)propenal were added. The mixture was stirred at room temperature for 1.5 h and then refluxed for 10 h. During this time a yellow solid precipitated. The reaction mixture was diluted with water, and acidified with 10% HCl. The yellow solid was filtered off, washed with water, ethanol and diethyl ether and then with n-hexane. This afforded 2-hydroxy-5-(4-fluorophenyl)nicotinonitrile as a yellow solid. The above yellow solid product was added to a mixture of acetic acid and conc. HCl. The reaction mixture was refluxed for 18 h, diluted with water and cooled under stirring. The solid was filtered off, washed with water and 50% ethanol. This afforded 2-hydroxy-5-(4-fluorophenyl)nicotinic acid (HFPNA) as a light gray solid. ^{1}H NMR (300 MHz, $CDCl_3$) δ: 14.7 (brs, 1H, COOH), 8.59 (brd, J = 3.00 Hz, 1H, ArH), 7.65 (brd, J = 2.70 Hz, 1H, ArH), 7.31 (ddd, J = 11.70, 8.70 and 2.10 Hz, 2H, ArH), 7.02 (t, J = 8.70, 8.40 Hz, 2H, ArH).

2.2. Materials

2HP was obtained from Aldrich Chemical Company (USA) and used as received and SA was obtained from SRL, India and used after repeated crystallization from MeOH. Spectroscopic grade solvents such as n-hexane (HEX), methylcyclohexane (MCH), acetonitrile (ACN), tetrahydrofuran (THF), dioxane (DOX), chloroform ($CHCl_3$), n-butanol (BuOH), iso-propanol (iPrOH), and methanol (MeOH) were purchased from Spectrochem (India) and used after proper distillation. Sulfuric acid (H_2SO_4), sodium hydroxide (NaOH), triethylamine (TEA), trifluoroacetic acid (TFA), phosphoric acid (H_3PO_4) and ethanol (EtOH) were obtained from E-Merck and used as received. Triple distilled water was used for preparing aqueous solutions.

2.3. Instrumentations and procedures

The absorption and emission measurements were done by Hitachi UV-Vis U-3501 spectrophotometer and Perkin-Elmer LS-50B spectrophotometer, respectively. In all measurements the sample concentration was maintained in the micromolar range in order to avoid aggregation and reabsorption effects. All spectral measurements have been carried out with freshly prepared solutions at ambient temperature of 27 °C, unless otherwise specified.

Fluorescence lifetimes were obtained from a Time-Correlated Single Photon Counting (TCSPC) spectrometer (time-resolution = 1.2 ns) using nanoLED-07 (IBH, UK) as the light source at 280 and 340 nm to trigger the fluorescence of HFPNA The observed fluorescence intensities were fitted by using a non-linear least-squares fitting procedure to a function ($X(t) = \int_0^t E(t')R(t-t')\,dt$) comprising the convolution of the IRF ($E(t)$) with a sum of exponentials ($R(t) = A + \sum_{i=1}^{N} B_i\, e^{t/\tau_i}$) with pre-exponential factors (B_i), characteristic lifetime (τ_i) and a background (A). Relative contribution of each component was obtained from a biexponential fitting finally was expressed by the following equation:

$$a_n = \frac{B_n}{\sum_{i=1}^{N} B_i} \tag{1}$$

The quality of the fits have been assessed over the entire decay range, including the rising edge, and tested with a visual inspection of the residuals of the fitted functions to the actual data and other statistical parameters, e.g. χ^2 criteria and Durbin–Watson (DW) parameter. A value of χ^2 close to unity and value of DW >1.8 ascertain quality fit obtained in each case.

The mean (average) fluorescence lifetimes for the decay curves were calculated from the decay times and the relative contribution of the components using the following equation [10]:

$$\langle\tau\rangle = \tau_{\text{avg}} = \frac{\sum_i a_i \tau_i^2}{\sum_i a_i \tau_i} \tag{2}$$

Solutions of definite pH values were prepared (by varying the composition of H_3PO_4 and NaOH in water) by Systronics μpH System 361 pH-meter.

2.4. Theoretical calculations

Theoretical calculations have been performed to calculate structures and potential energy surfaces along the isomerisation coordinates according to the "*distinguished coordinate approach*" [10,40,41]. The ground state structures for all the possible conformations were computed using Hartree–Fock (HF) and DFT methods by GUASSIAN 03 suit of programme [42]. Excited-state structure of lactim-form has been optimized at CIS level and the geometry of the lactam-form has been optimized by fixing the O_d–H distance (here O_7–H_8 bond in Chart 1) at $N_a\cdots H$ distance (here $N_3\cdots H_8$ distance in Chart 1) at HF level, since for otherwise the more stable lactim-form will be reverted back in calculation [10]. Ground state intramolecular proton transfer (GSIPT) curves were elucidated using the energies of the B3LYP/6-31G** fully optimized geometry at fixed O_d–H distances over the range of 0.95–1.8 Å. The excited-state potential energy curves (PECs) were obtained by

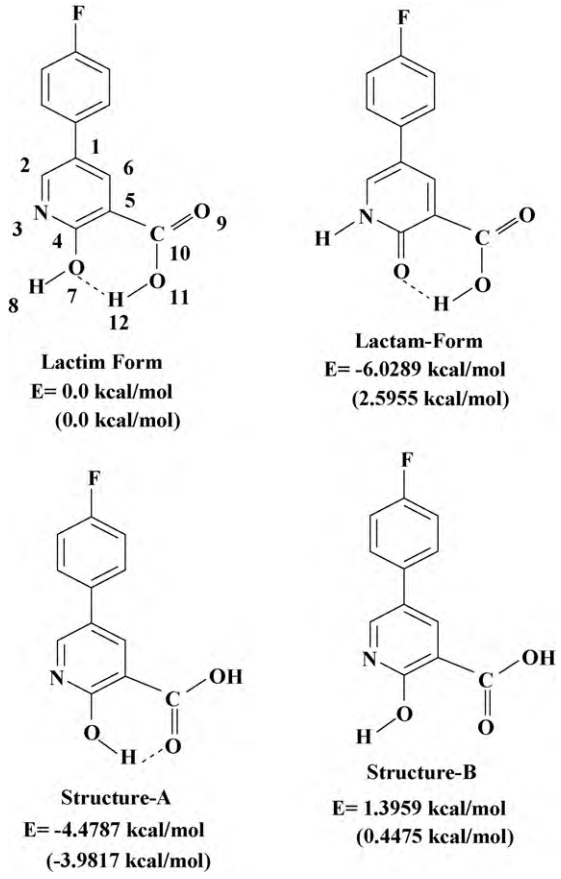

Chart 1. Schematic of computed ground state low energy structures of HFPNA obtained by DFT//B3LYP/6-31G** method (energies with respect to lactim-form are given and the values within parenthesis indicate energies at HF/6-31G** level).

calculating the Franck-Condon transition energies for the B3LYP/6-31G** ground state optimized structures at fixed O_d–H distances at the TDDFT/6-31G** level. The Franck–Condon curves for the proton transfer process were generated by adding the TDDFT/6-31G** excitation energies to the corresponding GSIPT curves. This type of approach has been successfully reported in several recent papers for studying ESIPT reaction [4,10,40,41,43].

3. Results and discussions

3.1. Absorption study

Structurally HFPNA molecule has two basic units capable for exhibiting proton transfer reaction and these are well studied systems – 2-hydroxypyridine (2HP) and salicylic acid (SA). Therefore it is worth to discuss spectral properties of SA and 2HP briefly. In all solvents, 2HP exhibits two absorption bands – one at the range of ~227–230 nm and another at ~297–305 nm [17] (Figure S1, Table S1 of Supplementary Information [44]). A large number of reports on the tautomerisation reaction between 2HP ↔ 2PY confirm about the presence of two stable tautomeric forms, the lactim-form (2HP) and the lactam-form (2PY) in the ground state [13–21,24,29,45–48]. Comparing the observed spectra in different solvents (Figure S1) with available data and considering the magnitude of the barrier height, the shorter wavelength and the longer wavelength absorption bands have been assigned to 2HP and 2PY, respectively [17,29].

In case of salicylic acid, a broad and structureless absorption band appears at 300–312 nm wavelength region (Figure S2, Table S1 of Supplementary Information [44]) due to π–π^* transition

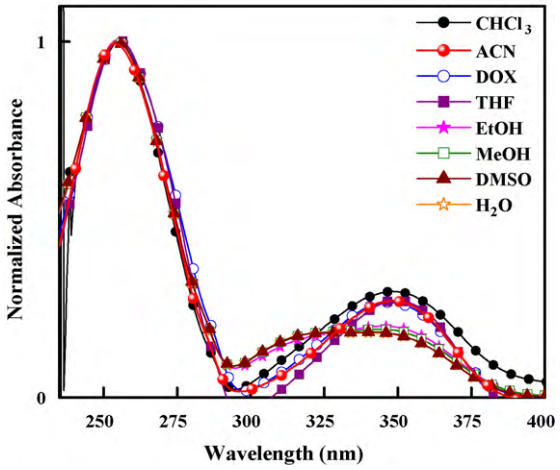

Fig. 1. Normalized absorption spectra of HFPNA in different media ([HFPNA] = 1.5–2.0 μM).

of the closed conformer of SA (Scheme S1 of Supplementary Information [44]). Bisht et al. studied the excitation spectra of SA under supersonic nozzle expansion condition and found the S_0–S_1 transition origin at 335.34 and 311.52 nm which are assigned to the closed conformer of SA and its rotamer, respectively (Scheme S1) [38]. In condensed phase spectra, however, we did not observe such two distinctly resolved bands due to the possibility of overlapping of rotamer absorption band within the broad band. Solute–solvent interaction in solution may be responsible for such broadening of the spectrum.

Fig. 1 and Table 1 display the absorption spectra and the corresponding spectroscopic parameters for HFPNA recorded in different solvents at room temperature. (The absorption spectra in Fig. 1, S1 and S2 have been normalized with respect to peak absorbance so as to allow a clear visual comparison of the absorption maxima positions. The actual absorbance values are not of much significance here.) As seen in the figure, HFPNA exhibits two absorption bands – one at ~250 nm and another at ~350 nm. A direct comparison reveals that the appearance and shape of the absorption spectra of HFPNA are closure to those of 2HP while are distinctly different from those of SA. Hence, the ~250 and ~350 nm absorption bands are assigned to the lactim-form and lactam-form of HFPNA, respectively (Scheme 1). Additionally, a hump is observed at ~317 nm only in polar protic solvents; with 2HP, however, no additional hump was observed in protic media. This may be due to the anionic species produced upon deprotonation of the –COOH group of HFPNA (Scheme 1). However, the possibility of formation of intermolecular hydrogen bonded clusters of HFPNA with protic

Table 1
Spectroscopic parameters of HFPNA obtained from absorption and emission spectra in different solvents at room temperature.

Solvent	Absorbance		Emission, λ_1 (nm)	Quantum yield, Φ_f
	λ_1 (nm)	λ_2 (nm)		
MCH	275	384	422	0.113
HEX	273	384	420	0.112
$CHCl_3$	256	349	422	–
ACN	252	349	415	0.235
DOX	255	348	419	–
BuOH	255	352	419	0.511
iPrOH	255	352	419	0.462
EtOH	255	317, 351	419	0.451
MeOH	255	317, 353	415	0.260
Water	256	334	424	0.159
DMSO	262	353	413	–

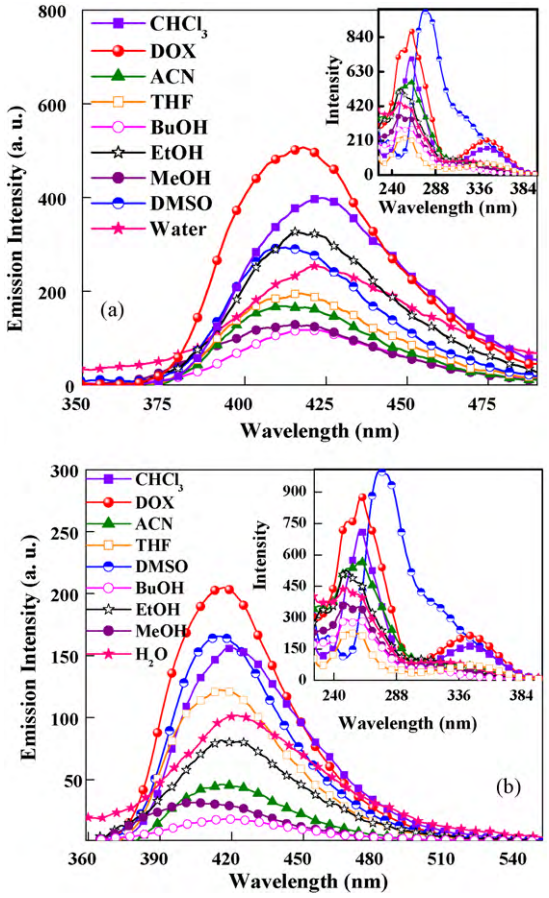

Fig. 2. Fluorescence emission spectra of HFPNA (1.5–2.0 μM) in different media: (a) λ_{ex} = 255 nm and (b) λ_{ex} = 350 nm. Insets show the excitation spectra.

solvents cannot be ruled out at this stage. Also a slight blue shift of the lower energy absorption band of HFPNA in water (from ~350 to ~335 nm) may be due to deprotonation of the –COOH group in neutral water as deprotonation of –COOH functional moiety is known to give rise to blue shifted absorption [49].

3.2. Emission and excitation study

The emission spectra of 2HP in different solvents are displayed in Figure S3 and the results are collected in Table S1 of Supplementary Information [44]. The most interesting feature in the emission properties of 2HP is that excitation at either of the two absorption maxima produces emission maxima at the same position. This is explained as follows: excitation at λ_{abs}^{max} of 2PY-form (lower energy band) shows the local emission of 2PY. But excitation at λ_{abs}^{max} of 2HP (higher energy band) too produces the local emission of 2PY and not of 2HP, because the process of emission in this case is supposed to be preceded by an ultrafast PT process in the excited state. A schematic presentation of the phenomenon is given in Scheme S2 of Supplementary Information [44]. On the other hand, SA exhibits distinct dual emission in all solvents (Figure S4 of Supplementary Information [44]). The higher energy emission band is due to the rotamer of SA while the large Stokes shifted band is attributed to the PT-form [10,38] (Scheme S1 of Supplementary Information [44]).

Fig. 2a and b illustrates the emission spectral profiles of HFPNA as assayed in different solvents at room temperature and the relevant spectroscopic parameters are compiled in Table 1. As seen in the figures, excitation at either of the two absorption maxima of HFPNA leads to no change in the position of the emission maxima. No dual emission is observed for HFPNA and the spectral characteristics are noticeably parallel to those of 2HP while at the same time the differences with SA are also prominent. The well-known dual emission of SA is explained on the basis of the presence of two conformers viz., closed form and the rotamer (Scheme S1) of which the former is capable of undergoing ESIPT [10,31]. But the lack of dual emission in HFPNA hints the absence of similar type of closed conformer and rotamer as in SA, rather the emission spectral profile of HFPNA can be explained according to Scheme 1 (which parallels to Scheme S2 of Supplementary Information [44]), i.e. excitation at the longer wavelength (λ_{ex} ~350 nm, lactam-form of HFPNA) produces the local emission of the lactam-form only. But following excitation at the shorter wavelength (λ_{ex} ~250 nm, lactim-form of HFPNA) also, the local emission of the lactam-form is obtained due to the operation of an ultrafast lactim- to lactam-changeover on the excited-state surface.

Insets of Fig. 2 reveal that the excitation spectra obtained in all solvents assayed are authentic replicates of the corresponding absorption spectra indicating that the origin of the lactam-form emission is through excitation of the lactim-form, i.e. the aforementioned interpretation of emission characteristics of HFPNA in connection with resemblance to those of 2HP is taken over a reinforcing avenue through the excitation spectral properties of HFPNA.

3.3. Spectral modulations as a function of variation of medium-pH

The pH variation experiments on the absorption and emission spectral profiles resulted in some interesting modulations which emerge to play vital roles in construing the ground- and excited-state photophysics of HFPNA with a deeper insight. A careful scrutiny of the spectral modifications with pH-change leads us to unravel the presence of different absorbing and emitting species in solution under various circumstances.

Upon addition of NaOH to a methanolic solution of HFPNA, the ~317 nm hump is found to persist and experience an increment in absorbance, while the ~350 nm band disappears (Fig. 3a). At the same time as seen in Fig. 3b, addition of sulfuric acid to a methanolic solution of HFPNA results in a reverse effect, i.e., suppression of the ~317 nm hump and persistence of only ~350 nm band. This observation is in line with previous assignment that the ~317 nm hump is more likely to be due to the anion (rather than hydrogen bonded clusters) which thus disappears in the presence of acid and persists in basic medium whereas the neutral form is responsible for the ~350 nm band (Scheme 2).

Similar observations are found for addition of acid TFA and base TEA in a polar aprotic solvent ACN (Fig. 4a and b). The hump at ~317 nm (anion, Scheme 2) in ACN is, however, generated only after addition of TEA. Furthermore, addition of TEA to an ACN solution of SA generates the anion band at ~300 nm (Figure S5 of Supplementary Information [44]); this is close to 317 nm of HFPNA. Thus it seems safe to conclude that ~317 nm absorption band of HFPNA is attributable to the anionic species formed upon deprotonation of the –COOH group. Whereas, addition of base (OH^- or TEA) to 2HP has been found to cause no significant changes at all (figures not given), which may be due to repulsive interaction between the localized lone pair on N-atom of 2HP and the negative charge of OH^- anion. That the –COOH group might be ionized in neutral water is again supported by the fact that in the presence of dilute sulfuric acid the ~335 nm band in aqueous medium shifts to ~350 nm (Fig. 5) which is ascribed to the neutral species (Scheme 2).

As in case of absorption spectra, the pH induced modifications of the emission profile of HFPNA are also noteworthy. Fig. 6a reveals the red shift of emission maxima along with intensity enhancement with decrease of pH of a methanolic solution of HFPNA. On the other hand, increase of pH leads to intensity enhancement coupled with blue shift of the emission maxima (Fig. 6b). Such consistent shift-

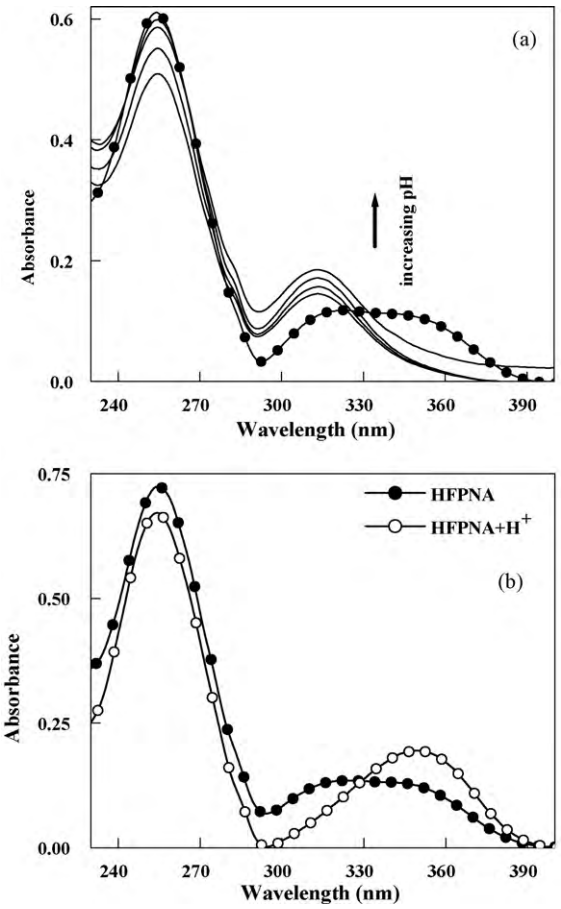

Fig. 3. Effect of variation of pH on the absorption profile of HFPNA (1.5–2.0 μM) in methanolic medium: (a) increasing pH (addition of base (NaOH)) and (b) decreasing pH (addition of acid (H_2SO_4)).

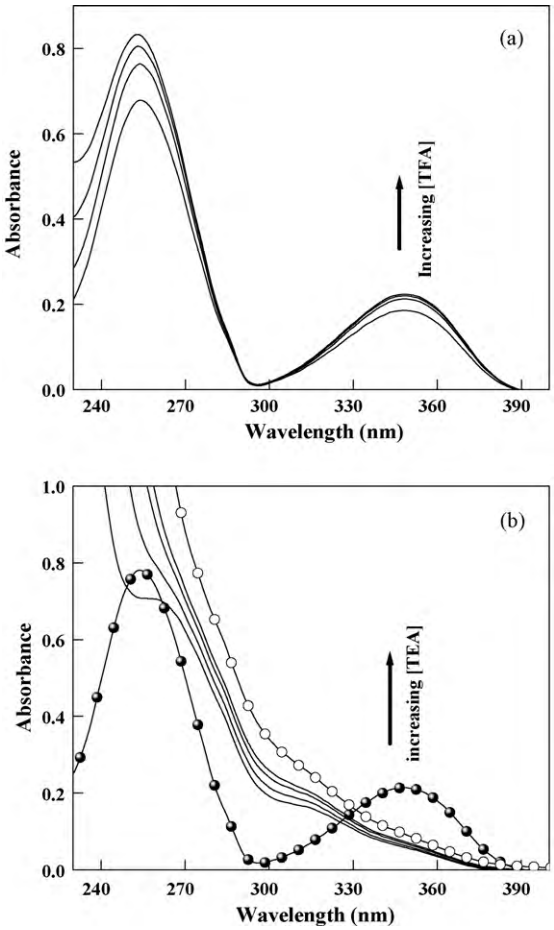

Fig. 4. Effect of addition of (a) acid (TFA) and (b) base (TEA) on the absorption spectra of HFPNA (1.5–2.0 μM) in aprotic (ACN) medium.

ing of the emission maxima positions with variation of pH seems to reinforce the assignments of pH variation experiments on the absorption profile. In protic solvent the –COOH group may remain ionized and with decrease of pH the neutral species is formed whereas in an alkaline solution the –OH proton is also likely to undergo ionization producing a dianionic species (Scheme 2). The insets of Fig. 6a and b depict the excitation spectra with pH variation which are found to be in excellent agreement with absorption spectra, i.e., a hump at ~309 nm (due to anion) is found in pure MeOH but disappears in acidic pH leaving only the ~345 nm band (due to the neutral species). Similarly in alkaline pH the ~345 nm band disappears and the band at ~309 nm (due to anion) persists. Very similar observations are found for pH variation experiments in a polar aprotic solvent (ACN) also (figures not given).

The observation of considerable intensity enhancement with variation of pH afforded us the impetus to go into the search for any correlation between the magnitude of emission intensity variation and pH of the medium so as to verify the possibility of exploiting HFPNA as a pH sensor. For this purpose the emission spectra of HFPNA have been recorded in a series of solutions of varying pH (prepared from varying the composition of H_3PO_4 and NaOH) and the magnitudes of emission intensity are plotted as a function of pH (Fig. 6c). The obtention of a linear regression points towards the probability that HFPNA can be employed as a sensor to determine

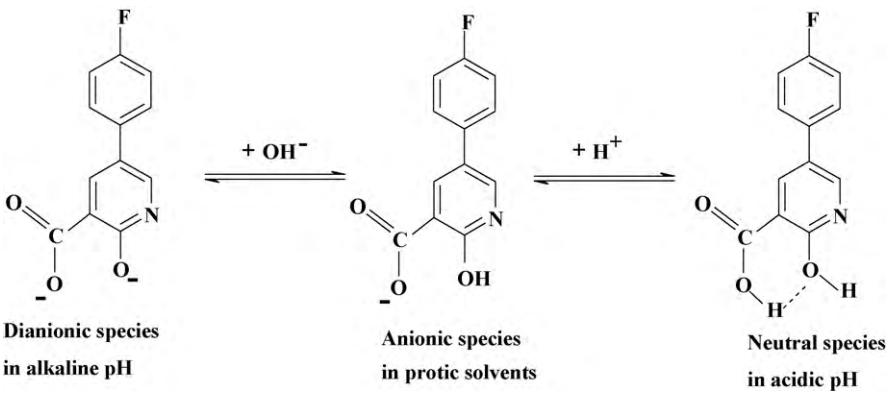

Scheme 2. Protonation/deprotonation reaction in HFPNA as a function of pH of the medium.

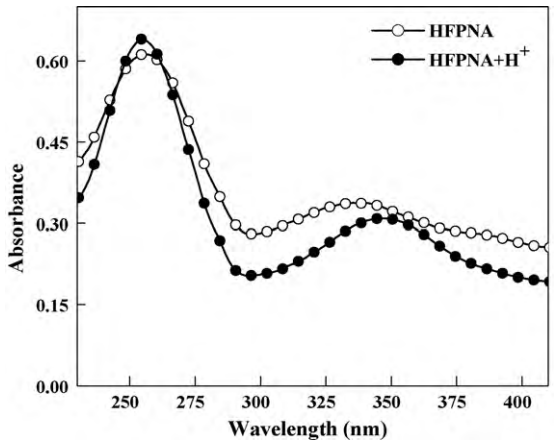

Fig. 5. Effect of addition of acid (H_2SO_4) on the absorption spectra of HFPNA (1.5–2.0 μM) in aqueous medium.

the pH of the medium. However, that at higher pH the linearity is lost seems attributable to the complicacies of situation as an alkaline pH may induce the formation of dianionic species.

3.4. Fluorescence quantum yield measurements

The fluorescence quantum yields of the PT species of all three compounds studied have been estimated in solvents of different polarities using secondary standard method. Bovine Serum Albumin (λ_{abs} ~280 nm and Φ_f = 0.13 in Tris–HCl buffer of pH = 7.4) is the secondary standard for 2HP and SA and for HFPNA this purpose is served by anthracene (λ_{abs} ~350 nm and Φ_f = 0.27 in MeOH). The quantum yield values have been calculated on the basis of the following equation [40,43,50,51]:

$$\Phi = \Phi_S \frac{I \cdot OD_S \cdot \eta^2}{I_S \cdot OD \cdot \eta_S^2}$$

where η is refractive index of the medium, OD is absorbance, I is area under the fluorescence curve and Φ is quantum yield and subscript "S" stands for the corresponding parameters of the secondary standard. The calculated values of quantum yields of the PT species in different solvents at room temperature for all three compounds have been tabulated in Table 1 (HFPNA) and S1 (2HP and SA). The quantum yields are found to be quite appreciable and this observation seems to receive good theoretical verification from the magnitude of the computed oscillator strength in the excited state, which is quite high for the lactam (PT) form in comparison to that for the lactim-form (Section 3.6). Additionally, for polar protic solvents the quantum yield values are seen to be reduced with increase in H-bonding efficiency of the solvents. This observation is rationalized on the ground that increased efficiency of intermolecular H-bonding between solute and solvent accompanies with it the activation of radiationless decay channels which in turn induces reduction on radiative decay route as manifested through consequent lowering of quantum yields [40,43].

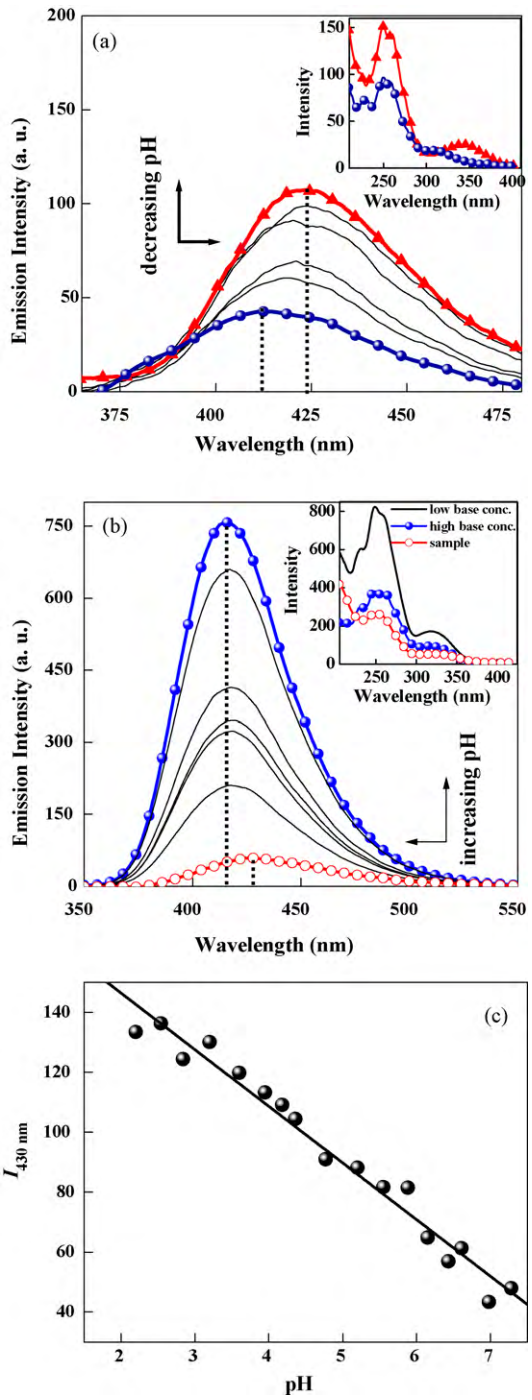

Fig. 6. Effect of variation of pH on the emission profile (λ_{ex} = 350 nm) of HFPNA (1.5–2.0 μM) in methanolic medium: (a) decreasing pH (addition of acid (H_2SO_4)) and (b) increasing pH (addition of base (NaOH)). (c) Plot of emission intensity ($I_{430\,nm}$) of HFPNA as a function of pH of the medium (λ_{ex} = 350 nm).

3.5. Fluorescence lifetime measurements

Because of its inherent sensitivity towards excited-state affairs, fluorescence lifetime measurements have long been recognized as a sensitive indicator of the local environment of a fluorophore, apart from being applied in monitoring sensitive issues like differential degrees of solvent relaxation around a fluorophore, presence of more than one chemical entity in a solution and so forth [10,40,43]. The supreme sensitivity of this technique has acquired it a position of enormous significance and erudition in the realm of photochemistry whence with a view to fathom deeper into the excited-state photophysics of HFPNA, fluorescence lifetime has been measured. The molecule is excited at λ_{ex} = 280 and 340 nm with a view to excite the lactim- and lactam-forms, respectively (ideally the lactim and lactam-forms should have been excited at λ_{ex} ~250 and 350 nm respectively, but we were restricted by the limitations of the available light sources). The time-resolved fluorescence decay profiles in polar aprotic medium ACN (Fig. 7a) are best fitted to monoexponential functions as evident from the data compiled in Table 2. For λ_{ex} = 340 nm it is reasonable to presume that the

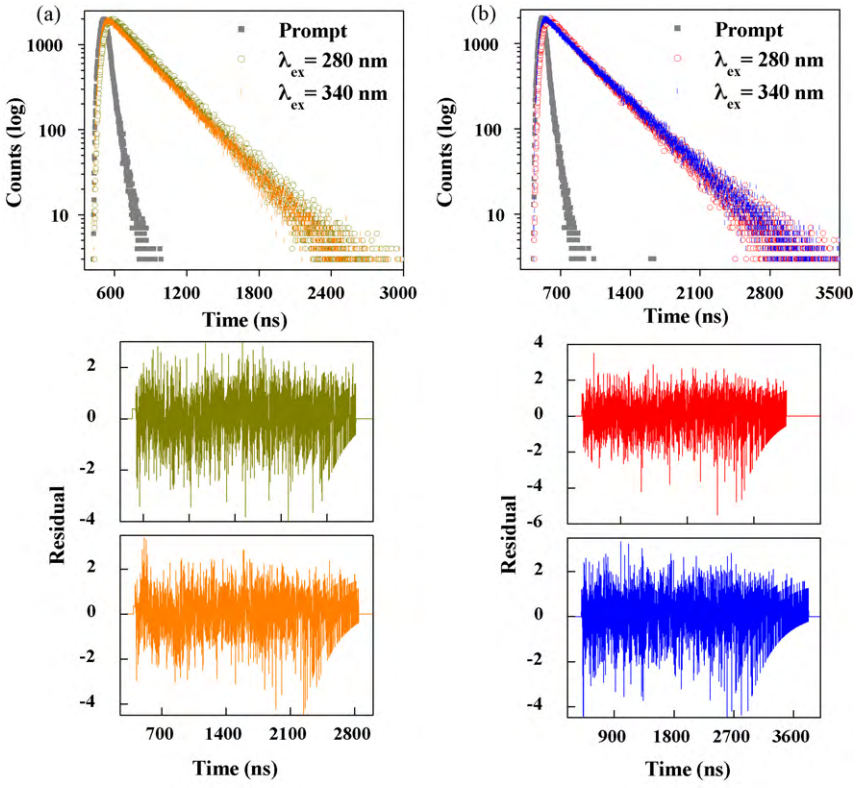

Fig. 7. Time-resolved emission decay profile of HFPNA in (a) ACN (λ_{em} = 415 nm) and (b) MeOH (λ_{em} = 415 nm). The excitation wavelengths (λ_{ex} = 280 nm and λ_{ex} = 340 nm to trigger the fluorescence of lactim and lactam forms, respectively) are indicated in the figure legends. The lower panel shows the residual plot of the fitted functions to the respective data.

lactam-form is selectively excited since the lactim-form does not absorb at this wavelength (Fig. 1; Section 3.1) when the corresponding time-constant conform to the excited-state lifetime of the lactam-form. However, we encountered a more crucial observation during monitoring the excited-state fluorescence lifetime of HFPNA in ACN solvent at λ_{ex} = 280 nm which leads to a monoexponential decay pattern with a lifetime value intimately comparable to that obtained in the previous case. This result seems to strongly substantiate our steady-state spectral findings in the sense that upon selectively exciting the lactim-form (λ_{ex} = 280 nm; the lactam-form does not absorb at the higher energy wavelength, see Fig. 1 and Section 3.1) the resultant excited-state lifetime corroborates to that of the lactam-form. This result can be readily connected to the operation of an ultrafast ESIPT (lactim → lactam) process over the excited-state PES. However, it is ethical to point out that ideally a sequential kinetics should have been observed with a rising component for the lactam-form having a time-constant comparable in magnitude to that corresponding to the decay component of the lactim-form. This sort of an observation would have established the occurrence of an ultrafast lactim → lactam transformation on the PES beyond doubts. That we are not fortunate enough to comply with such an observation seems attributable to the limitation of the time-resolution of our instrument (1.2 ns). Indeed, it is not irrational to consider that the lactim-form is endowed with an ultrafast excited-state lifetime in view of the fluorescence decay characteristics of the parent molecule 2HP, as mentioned below.

An attempt to measure the fluorescence lifetime in a protic solvent (MeOH), however, appeared with a little more complicacy in form of a biexponential decay pattern (for both λ_{ex} = 280 and 340 nm) with a major contributing slower component and a short-lived minor component (Fig. 7b, Table 2). Since the time-constant for the slower component (major) is strikingly similar for each choice of excitation wavelength (280 and 340 nm) and is comparable to that for excited-state lifetime of the lactam-form obtained in ACN, it seems justified to ascertain the corresponding time-constant to the lactam-form. Obtention of a biexponential decay might seem a little puzzling at the first glance, but is interpreted with attention to protic character of the solvent which can thereby induce the formation of solute–solvent intermolecular hydrogen bonded clusters and/or anion of HFPNA which is subsequently becoming responsible for the short-lived minor component. A detailed analysis of the steady-state spectral properties of HFPNA in foregoing sections strongly substantiates such possibilities (Sections 3.1 and 3.3). Indeed, the substantial impact of solute–solvent intermolecular hydrogen bonding interactions on the fluorescence decay properties of fluorophores are quite well

Table 2
Fluorescence lifetimes of HFPNA in different solvents at room temperature.

Medium	λ_{ex} (nm)	τ_1 (ns)	τ_2 (ns)	a_1 (%)	a_2 (%)	τ_{avg} (ns)	χ^2	DW[a]
ACN	280	3.977	–	100.0	–	–	0.99	1.95
ACN	340	3.973	–	100.0	–	–	1.00	1.93
MeOH	280	5.242	1.848	74.1	25.9	4.870	1.00	1.93
MeOH	340	5.357	1.343	83.1	16.9	5.162	1.03	1.98

[a] Durbin–Watson parameter.

known and profusely discussed in the literature [52,53]. Thus the steady-state and time-resolved spectral assignments seem to be efficient complements of each other in construing the photophysics of the studied molecule. Additionally, the present findings also advocate for the commendable sensitivity of the technique of fluorescence lifetime measurement towards excited-state interactions by virtue of which the impact of solute–solvent interaction on the photophysics of HFPNA is also indicated (differential decay behaviour in polar aprotic and protic media).

Unfortunately a direct comparison of the lifetime data of HFPNA with those of SA and 2HP was prohibited because of the extremely fast decay of 2HP falling beyond the measuring limit of the instrument. Typical decay profiles with corresponding fitting parameters for SA are provided in the supplementary information [44] (Figure S6 and Table S2).

3.6. Theoretical calculation

3.6.1. Structures, energies and changes in geometrical parameters during ESIPT reaction

Conformational landscapes of HFPNA molecule are explored in the electronic ground state by Density Functional Theory (DFT) method using B3LYP hybrid functional and 6-31G** basis set and the structural parameters for the lactim and lactam-forms are presented in Table 3. We have also calculated the structures, energies of different forms of HFPNA at HF level of theory, employing the same 6-31G** basis set so that comparison of the results of two theoretical methods does not suffer from the shortcomings due to change of basis set. Schematic of different low energy computed structures with respect to the position of the hydroxyl and carboxyl groups for the ground state are shown in Chart 1. Out of four possible structures, three have stabilizing intramolecular hydrogen bond, the lack of which is making structure-B a high energy conformer. Although, calculations at either level of calculation (DFT or HF) predicts the intramolecularly hydrogen bonded structure-A (six member H-bond) to be the lowest energy conformer in the ground state, but, our experimental results point towards the existence of two conformers viz., lactim- and lactam-forms at the ground state. Therefore, for further calculation we shall start with the lactim-form.

The changes in the structural parameters (Table 3) as a result of transition from the ground state (GS) to the excited state (ES), such as increase of O_7–H_8 bond length from 0.9474 Å to 0.9482 Å, decrease of N_3–O_7 distance from 2.2501 Å to 2.2498 Å and decrease of $\angle N_3$–H_8–O_7 bond angle from 78.133° to 77.570° support the possibility of translocation of the proton from O_7 to N_3 in the ES. Additionally, the process of ESIPT should result in increment of double bond character of C_4–O_7 bond with simultaneous decrement of the same in N_3–C_4 bond, as manifested in the corresponding bond distances (Table 3).

Examination of the computed negative charge distribution according to Mulliken scheme at HF/6-31G** level reveals an increase in negative charge distribution on N-atom (from −0.643 in GS to −0.649 in ES) with simultaneous decrease of the same on O-atom of OH group (from −0.681 in GS to −0.672 in ES) from ground to the excited state. Such modulation of electronic charge density stand in line with translocation of the proton following photoexcitation [40,43]. It is probable that on excitation HFPNA attains a delocalized state, which then relaxes to the proton transferred configuration with the transfer of the proton from –OH group to the ring N-atom.

3.6.2. Elucidation of potential energy curve (PEC) for ESIPT reaction in HFPNA

A more vivid insight into the mode of tautomerisation reaction in HFPNA can be obtained from the examination of the PEC across both the probable PT pathways. In fact, the most critical assessment of an intrinsic proton transfer process occurring within a molecule can be achieved by scrutiny of PEC across the reaction coordinate. At a first glance ESIPT reaction in HFPNA was expected to occur via the route that resemble that of SA because of its involvement with a more stable six member H-bond, although the experimental

Table 3
Relevant structural parameters for the optimized ground and excited states of HFPNA at HF and CIS levels and at DFT level with B3LYP hybrid functional and 6-31G** basis set.

Parameters[a]	HF level			DFT level/B3LYP	
	Lactim-form		Lactam-form	Lactim-form	Lactam-form
	GS	ES	GS	GS	GS
N_3–C_4	1.296	1.306	1.359	1.325	1.400
C_4–C_5	1.397	1.442	1.446	1.407	1.428
C_5–C_{10}	1.502	1.491	1.499	1.506	1.501
C_{10}–O_{11}	1.320	1.323	1.314	1.345	1.340
O_{11}–H_{12}	0.947	0.946	0.956	0.974	0.988
H_{12}–O_7	1.874	1.885	1.842	1.815	1.690
H_8–O_7	0.947	0.948	–	0.971	–
C_4–O_7	1.341	1.336	1.214	1.363	1.234
N_3–H_8	–	–	0.995	–	1.026
N_3–O_7	2.250	2.249	2.067	2.283	2.093
$\angle N_3$–C_4–O_7	116.440	117.505	117.123	116.219	114.830
$\angle C_4$–C_5–C_{10}	126.316	126.843	121.485	126.125	119.289
$\angle C_5$–C_{10}–O_{11}	118.329	118.473	116.449	117.821	115.146
$\angle C_{10}$–O_{11}–H_{12}	113.166	113.00806	111.986	110.882	110.820
$\angle O_{11}$–H_{12}–O_7	142.314	142.640	146.616	145.845	151.473
$\angle C_4$–O_7–H_8	108.855	108.83713	–	106.988	–
$\angle C_4$–O_7–H_{12}	100.242	101.082	95.533	99.882	87.473
$\angle H_8$–N_3–C_4	–	–	109.235	–	106.748
$\angle N_3$–H_8–O_7	78.133	77.570	100.606	79.659	101.037
$\angle N_3$–C_4–O_7–H_8	−0.059	0.115	–	−0.046	–
$\angle N_3$–C_4–O_7–H_{12}	179.714	−179.026	179.779	−179.661	−178.175
$\angle O_7$–H_{12}–O_{11}–C_{10}	−0.720	0.182	−0.379	0.462	−0.187
$\angle O_{11}$–C_{10}–C_5–C_4	0.997	−0.634	0.076	−0.344	−0.289
$\angle O_{11}$–H_{12}–O_7–C_4	0.997	−0.634	0.536	−0.702	−7.627

[a] Bond lengths in Å and angles in degree (°).

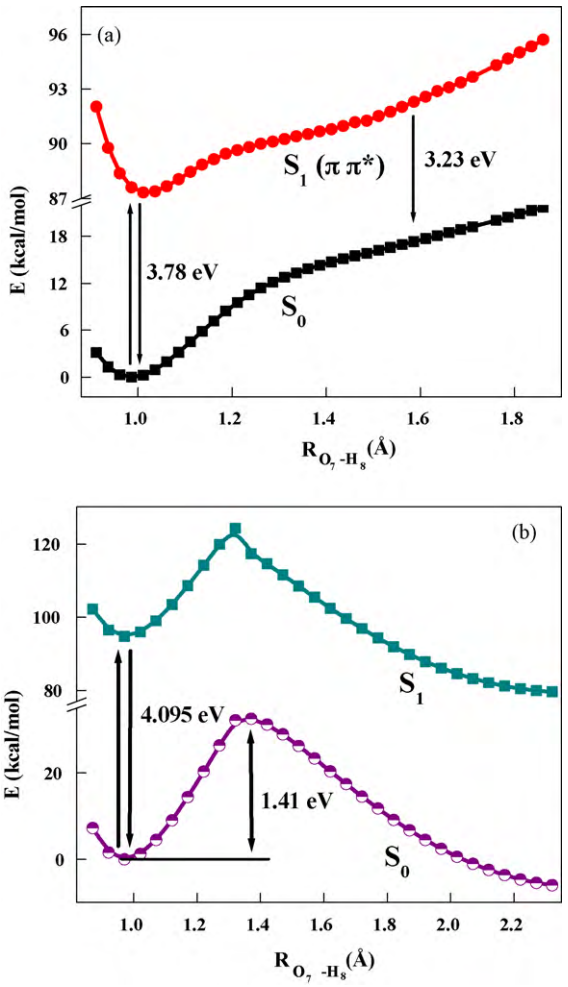

Fig. 8. Potential energy curves for S_0 and S_1 states along the proton transfer coordinate of HFPNA according to (a) Scheme S1 and (b) Scheme S2. Calculations at DFT//B3LYP/6-31G** level for the S_0 state and at TDDFT(TD-B3LYP/6-31G**) level for S_1 state.

findings are in line with those of 2HP. At this point, theoretical calculations, more particularly the evaluation of PECs, have been exploited with a view to afford critical information for deciphering the photophysics of HFPNA.

For a better comparison, the PECs for SA and 2HP for the ESIPT reaction are constructed at the same level of calculation and given respectively in Figure S7 and S8 of Supplementary Information [44]. Fig. 8a and b displays the PECs of HFPNA for PT reaction according to Scheme S1 and S2 (in Supplementary Information [44]), respectively. Clearly, a comparison of the PECs reflects remarkable dissimilarities between HFPNA (Fig. 8a) and SA (Figure S7), but side-by-side the PECs in Fig. 8b (i.e. ESIPT reaction in HFPNA according to Scheme S2) happen to bear noticeable similarities with those of Figure S8 (2HP ↔ 2PY). The S_1 surface (Figure S7) for SA along the proton transfer coordinate predicts a barrierless process of ESIPT while the inoperativeness of a GSIPT process is dictated by the repulsive nature and high barrier height at the S_0 surface (also no minimum for the keto form at S_0 PEC). In HFPNA the operation of GSIPT (along the route depicted in Scheme S1) is negated based on similar arguments, i.e. repulsive nature of the S_0 surface coupled with considerably high magnitude of the energy barrier (Fig. 8a). But interestingly an ESIPT process (according to Scheme S1) in HFPNA also seems improbable following the qualitative similarity in appearance of the S_1 surface to the S_0 surface (Fig. 8a), i.e. carrying strong contradiction to the observations for SA

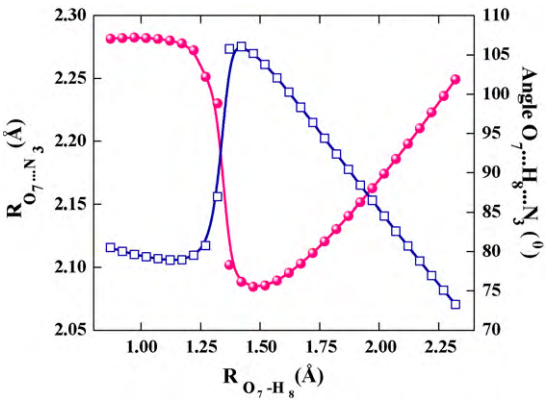

Fig. 9. Variation of $O_7\cdots N_3$ distance (pink circle) and $\angle O_7\cdots H_8\cdots N_3$ angle (blue square) with the proton transfer coordinate (O_7–H_8 bond axis) in the S_0 state (calculated at DFT/B3LYP/6-31G** level) in course of proton translocation in HFPNA according to Scheme S2.

(Fig. S7). The repulsive nature of the S_1 surface together with its high energy barrier and lack of minimum for the keto-form indicates the inoperativeness of an ESIPT reaction along this route (Scheme S1). Therefore, the theoretical results support our assignments of the experimental findings that in HFPNA, ESIPT reaction follows the route shown in Scheme S2, rather than that of Scheme S1.

In the above case, the PECs have been constructed by observing the change of energy along the reaction coordinate (RC), which in our case has been specified as to be the coordinate along which the proton undergoes translocation from O_7 to O_9 (as in structure-A of Chart 1)/N_3 (as in lactim-form of Chart 1), i.e. the $R_{O_7-H_8}$ distance. The $R_{O_7-H_8}$ distance was varied in 0.025 Å increment and the rest of the geometry was optimized for each choice of $R_{O_7-H_8}$ distance. Fig. 9 shows that the process of proton transfer also involves significant modulation of other geometrical parameters, mainly $\angle O_7\cdots H_8\cdots N_3$ angle and $O_7\cdots N_3$ distance, reflecting the inherent complex nature of the phenomenon. The figure dictates that midway through the proton transfer process the $O_7\cdots N_8$ length contracts to a minimum and the $\angle O_7\cdots H_8\cdots N_3$ angle increases to a maximum before relaxing to the lactam-form. A crossover point between lactim- and lactam-form is found at around O_7–H_8 distance of ~1.4 Å. This mirror image plot points towards the error that would be inevitably incorporated in the calculation by freezing all the coordinates during evaluation of the PEC.

Fig. 10a shows the three-dimensional potential energy surfaces (PESs) for the proton transfer reaction of HFPNA according to Scheme S2, i.e. change of energy with simultaneous variation of O_7–H_8 and $O_7\cdots N_3$ distances are depicted for both ground (S_0) and excited states (S_1) and Fig. 10b shows the PESs with simultaneous variation of O_7–H_8 and $O_7\cdots O_9$ distances, i.e. PT reaction of HFPNA according to Scheme S1. These results provide further confirmation to the conclusions derived from the analysis of Fig. 8, i.e. for PT reaction in HFPNA as per Scheme S1, the barrier still persists in the S_1 state as against the case of SA (Figure S11) while for a PT reaction according to Scheme S2, the PESs of HFPNA are strikingly similar to those of 2HP (Figure S11). Since the course of ESIPT reaction in HFPNA is already documented to strongly perturb other geometrical parameters like $\angle O_7\cdots H_8\cdots N_3$ angle and $O_7\cdots N_3$ distance, apart from O_7–H_8 bond, the three-dimensional PES (variation of energy with simultaneous variation of two important geometrical parameters viz. O_7–H_8 and $O_7\cdots N_3$ distances) stand as a strong complement for the two dimensional PECs.

Fig. 11 shows the variation of oscillator strength with $R_{O_7-H_8}$ distance on going from lactim-form to the lactam-form in the S_1 state. Enhancement of the calculated oscillator strength from lactim-form to the lactam-form on S_1 surface complies with the

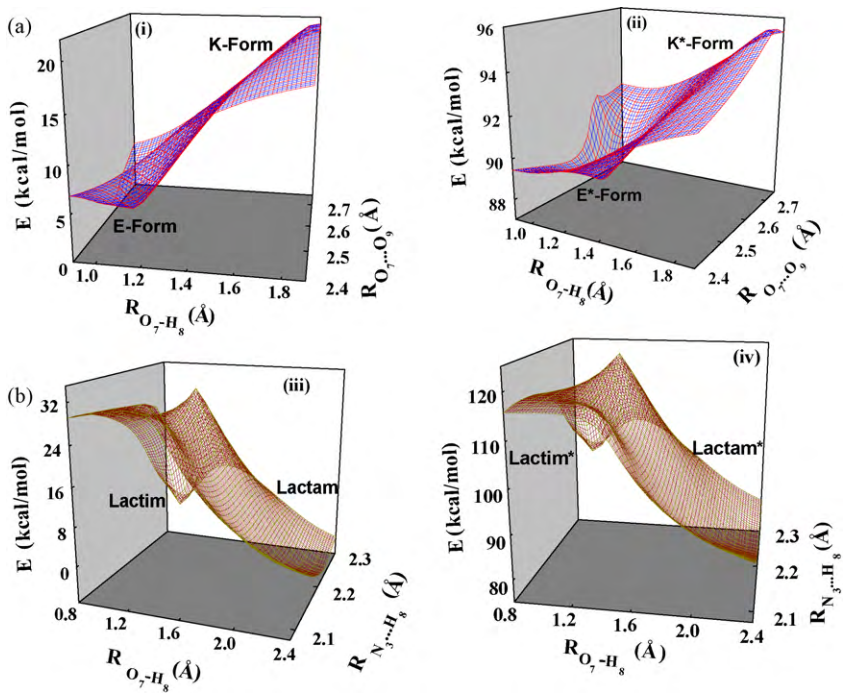

Fig. 10. Three-dimensional potential energy surfaces for proton transfer in HFPNA showing the variation of energy as a function of (a) O_7–H_8 and $O_7\cdots O_9$ distances according to Scheme S1 ((i) GS; (ii) ES) and (b) O_7–H_8 and $O_7\cdots N_3$ distances according to Scheme S2 ((iii) GS; (iv) ES).

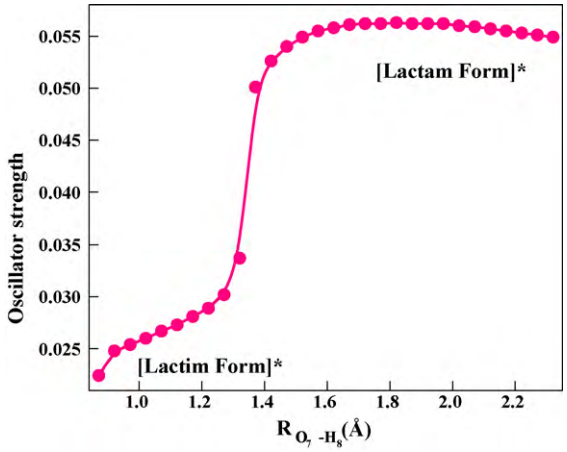

Fig. 11. Variation of the oscillator strength with O_7–H_8 distance in the S_1 state for ESIPT reaction according to Scheme S2 (at DFT/B3LYP/6-31G** level).

high fluorescence quantum yield of the proton transferred species (lactam-form) (as seen in Table 1).

4. Conclusion

In this paper, the photophysical properties of HFPNA have been investigated from experimental and theoretical perspectives on the basis of absorption, emission and time-resolved emission spectroscopy and quantum chemical calculations, respectively. The absorption and emission spectra of HFPNA are found to be similar to those of 2HP and distinctly different from those of SA. Spectral characteristics confirm the existence of lactim and lactam-forms in the ground state and excited-state lactim ↔ lactam tautomerisation reaction. Excitation of lactam-form produces its local emission whereas excitation of the lactim-form too shows emission of lactam-form, i.e., emission from lactim-form is supposed to be preceded by an ultrafast ESIPT reaction on the S_1 surface. Such emission spectral properties remarkably comply with those of 2HP and are not in agreement with those of SA which produces dual emission characteristic of a rotamer and the PT-form.

Theoretical calculations at DFT and HF levels predict the existence of intramolecularly H-bonded stable lactim and lactam-forms. The structural changes and charge distribution at the proton translocation site are found to be in favour of ESIPT reaction. Potential energy curves for an ESIPT reaction in HFPNA via the route that resemble to SA are found to be in strong incongruity with those of SA. In SA, the phenomenon of PT on the S_1 surface is a barrierless process whereas in HFPNA the barrier is quite high (∼0.08 kcal/mol at DFT/B3LYP/6-31G(d,p) level). Also it is found that the nature and shape of the S_1 surface in HFPNA is very similar to that of the S_0 surface, as against the case for SA. On the other extreme, PECs for an ESIPT reaction in HFPNA via the route that resemble to 2HP are similar in nature. Additionally, the presence of two tautomeric forms in the ground state is also verified in the lactim–lactam surface but not in the enol–keto surface.

In a nut-shell, the properties and the feasibility of proton transfer process and its mechanism in HFPNA in the excited and ground states inferred from the experimental data are well complemented from theoretical calculations.

Acknowledgements

N.G. acknowledges C.S.I.R., India (Project no. 01(2161)07/EMR-II) and D.S.T., India (Project no. SR/S1/PC/26/2008) for financial supports. B.K.P. and A.S. are also grateful to C.S.I.R., New Delhi for Senior Research Fellowship. Prof. T. Ganguly, Department of Spectroscopy, Indian Association for the Cultivation of Science, Jadavpur, Calcutta 700032, India is acknowledged for allowing us to use the TCSPC instrument for fluorescence lifetime measurements.

Appendix A. Supplementary data

Supplementary data associated with this article can be found, in the online version, at doi:10.1016/j.jphotochem.2010.06.028.

References

[1] K.Z. Weber, Phys. Chem. B 15 (1931) 18.
[2] T. Förster, Naturwissenschaften 36 (1949) 186.
[3] A. Weller, Discuss. Farady Soc. 27 (1959) 28, and references therein.
[4] J. Catalan, F. Fabero, M.S. Guijarro, R.M. Claramunt, M.D.S. Maria, M.C. Foces-Foces, F.H. Cano, J. Elguero, R. Sastre, J. Am. Chem. Soc. 112 (1990) 747.
[5] P.T. Chou, D. McMorrow, T.J. Aartsma, M. Kasha, J. Phys. Chem. 88 (1984) 4596.
[6] A.U. Acuna, A. Costela, J.M. Munoz, J. Phys. Chem. 90 (1986) 2807.
[7] R.M. Tarkka, X. Zhang, S.A. Jenekhe, J. Am. Chem. Soc. 118 (1996) 9438.
[8] A. Sytnik, I. Litvinyuk, Proc. Natl. Acad. Sci. U.S.A. 93 (1996) 12959.
[9] (a) A. Sytnik, M. Kasha, Proc. Natl. Acad. Sci. USA 91 (1994) 8627;
(b) D. Zhong, A. Douhal, A.H. Zewail, Proc. Natl. Acad. Sci. U.S.A. 97 (2000) 14056;
(c) A.S. Klymchenko, V.V. Shvadchak, D.A. Yushchenko, N. Jain, Y.J. Mely, J. Phys. Chem. B 112 (2008) 12050.
[10] S. Maheswari, A. Chowdhury, N. Sathyamurthy, H. Mishra, H.B. Tripathi, M. Panda, J.J. Chandrashekhar, J. Phys. Chem. A 103 (1999) 6257.
[11] M. Mosquera, J.C. Penedo, M.C.R. Rodriguez, F.J. Rodriguez-Prieto, J. Phys. Chem. 100 (1996) 5398.
[12] D.W. Chou, Y.H. Kim, M. Yoon, S.C. Jeoung, D. Kim, Chem. Phys. Lett. 226 (1994) 275.
[13] R.S. Brown, A. Tse, J.C. Vedaras, J. Am. Chem. Soc. 102 (1980) 1174.
[14] M.J. Cook, A.R. Katritzky, P. Linda, R.D. Tack, J. Chem. Soc., Perkin Trans. 2 (1972) 1295.
[15] P. Beak, F.S. Fry Jr., J. Am. Chem. Soc. 95 (1973) 1700.
[16] P. Beak, F.S. Fry Jr., J. Lee, F. Steele, J. Am. Chem. Soc. 98 (1976) 171.
[17] P. Beak, Acc. Chem. Res. 10 (1977) 186.
[18] A. Weisstuch, P. Neidig, A.C. Testa, J. Lumin. 10 (1975) 137.
[19] A. Fujimoto, K. Inuzuka, R. Shiba, Bull. Chem. Soc. Jpn. 54 (1981) 2802.
[20] O. Bensaude, M. Chevrier, J.-E. Dubois, J. Am. Chem. Soc. 101 (1979) 2423.
[21] C. Guimon, G. Garrabe, G. Pfister-Guillouzo, Tetrahedron Lett. 20 (1979) 2585.
[22] M.J. Nowak, L. Lapinski, J. Fulara, A. Les, L. Adamowicz, J. Phys. Chem. 96 (1992) 1562.
[23] A. Dikhissi, L. Houben, J. Smets, L. Adamowicz, G. Maes, J. Mol. Struct. 484 (1999) 215.
[24] J.S. Kwiatkowski, B. Szczodrowsla, Chem. Phys. 27 (1978) 389.
[25] A. Muller, F. Talbot, S. Leutwyler, J. Am. Chem. Soc. 124 (2002) 14486.
[26] C. Krebs, H.J. Hofmann, H.J. Kohler, C. Weiss, Chem. Phys. Lett. 69 (1980) 537.
[27] A. Lledos, J. Bertran, Tetrahedron Lett. 22 (1981) 775.
[28] H.-J. Hofmann, G. Peinel, C. Krebs, C. Weiss, Int. J. Quant. Chem. 20 (1980) 537.
[29] Y. Matsuda, T. Ebata, N. Mikami, J. Phys. Chem. A 105 (2001) 3475.
[30] M.K. Hazra, T. Chakraborty, J. Phys. Chem. A 110 (2006) 9130.
[31] D-l. Wu, L. Liu, G-f. Liu, D-z. Jia, J. Phys. Chem. A 111 (2007) 5244, and references therein.
[32] (a) A. Müller, F. Talbot, S. Leutwyler, J. Chem. Phys. 112 (2000) 3717;
(b) A. Müller, F. Talbot, S. Leutwyler, J. Chem. Phys. 115 (2001) 5192;
(c) A. Müller, F. Talbot, S. Leutwyler, J. Am. Chem. Soc. 124 (2002) 14486.
[33] I. Aikorta, J. Elguero, J. Org. Chem. 67 (2002) 1515.
[34] E.D. Raczynska, W. Kosinska, Chem. Rev. 105 (2005) 3561.
[35] P. Cieplak, P. Bash, U.C. Singh, P.A. Kollman, J. Am. Chem. Soc. 109 (1987) 6283.
[36] M.J. Scanlan, I.H. Hillier, A.A. MacDowell, J. Am. Chem. Soc. 105 (1983) 3568.
[37] (a) W.B. Parsons Jr., South Med. J. 56 (1963) 427;
(b) S. Tunaru, J. Kero, A. Schaub, C. Wufka, A. Blaukat, K. Pfeffer, S. Offermanns, Nat. Med. 9 (2003) 352;
(c) P.D. Boatman, J.G. Richman, G. Semple, J. Med. Chem. 51 (2008) 7653;
(d) A. Tamayo, C. Lodeiro, L. Escriche, J. Casabo, B. Covelo, P. González, Inorg. Chem. 44 (2005) 8105, and references therein;
(e) T. Asami, M. Baba, S. Yoshida, Biosci. Biotechnol. Biochem. 57 (1993) 350.
[38] (a) P.B. Bisht, H. Petek, K. Yoshihara, U. Nagashima, J. Chem. Phys. 103 (1995) 5290;
(b) F. Lahmani, A. Zehnacker-Rentein, J. Phys. Chem. A 101 (1997) 6141;
(c) L. Rodriguez-Santiago, M. Sodupe, A. Oiva, J. Bertran, J. Am. Chem. Soc. 121 (1999) 8882;
(d) A.L. Sobolewski, W. Domcke, J. Phys. Chem. A 108 (2004) 10917.
[39] Q.-S. Li, W.-H. Fang, J.-G. Yu, J. Phys. Chem. A 109 (2005) 3983.
[40] R.B. Singh, S. Mahanta, S. Kar, N. Guchhait, Chem. Phys. 331 (2007) 373.
[41] (a) R. de Vivie-Riedle, V.D. Waele, L. Kurtz, E. Riedle, J. Phys. Chem. A 107 (2003) 10591;
(b) J.A. Organero, M. Moreno, L. Santos, J.M. Lluch, A. Douhal, J. Phys. Chem. A 104 (2000) 8424.
[42] M.J. Frisch, et al., Gaussian 03, Revision B.03, Gaussian, Inc., Pittsburgh, PA, 2003.
[43] S. Mahanta, R.B. Singh, S. Kar, N. Guchhait, Chem. Phys. 324 (2006) 742.
[44] Supplementary Information.
[45] S. Tanabe, T. Ebata, M. Fujii, N. Mikami, Chem. Phys. Lett. 215 (1993) 347.
[46] M.R. Nimlos, D.F. Kelley, E.R. Bernstein, J. Phys. Chem. 93 (1989) 8732.
[47] H.I. Abdulla, E.F. El-Bermani, Spectrochim. Acta A 57 (2001) 2659.
[48] K. Sakota, S. Tokuhara, H. Sekiya, Chem. Phys. Lett. 448 (2007) 159.
[49] (a) T. Stalin, N. Rajendiran, J. Photochem. Photobiol. A: Chem. 182 (2006) 137;
(b) T. Stalin, N. Rajendiran, Chem. Phys. 322 (2006) 311.
[50] M. Maus, W. Rettig, D. Bonafoux, R. Lapouyade, J. Phys. Chem. A 103 (1999) 3388.
[51] M. Lukeman, D. Veale, P. Wan, V. Ranjit, N. Munaisinghe, J.E.T. Corrie, Can. J. Chem. 82 (2004) 240.
[52] J.R. Lakowicz, Principles of Fluorescence Spectroscopy, Plenum Press, New York, 1999.
[53] (a) Z. Grabowski, K. Rotkiewicz, W. Rettig, Chem. Rev. 103 (2003) 3899;
(b) R. Misra, A. Mandal, M. Mukhopadhyay, D.K. Maity, S.P. Bhattacharyya, J. Phys. Chem. B 113 (2009) 10779;
(c) A. Mallick, P. Putkayastha, N. Chattopadhyay, J. Photochem. Photobiol. C: Rev. 8 (2007) 109;
(d) A.-D. Gorse, M. Pesquer, J. Phys. Chem. 99 (1995) 4039;
(e) J. Seo, S. Kim, S.Y. Park, Am. Chem. Soc. 126 (2004) 11154;
(f) D. McMorrow, M. Kasha, J. Phys. Chem. 88 (1984) 2235;
(g) S.-L. Wang, J.-M. Lin, S.-E. Shu, C.-Y. Chern, Spectrochim. Acta Part A 210 (2010) 54;
(h) T. Yatsuhashi, Y. Nakajima, T. Shimada, H. Tachibana, H. Inoue, J. Phys. Chem. 102 (1998) 8657;
(i) K. Das, N. Sarkar, A.K. Ghosh, D. Majumdar, D.N. Nath, K. Bhattacharyya, J. Phys. Chem. 94 (1994) 9126.